RSC Advances

ROYAL SOCIETY OF CHEMISTRY

www.rsc.org/advances

Journal Name

COMMUNICATION

Facile synthesis of β-MnO_2/Polypyrrole nanorods and their enhanced lithium-storage properties†

Received 00th January 20xx,
Accepted 00th January 20xx

DOI: 10.1039/x0xx00000x

www.rsc.org/

Meng Wang[a], Qianxu Yang[a], Tiandong Zhang[a], Baokun Zhu[a]* and Guangda Li[b]*

In this work, β-MnO_2/polypyrrole (β-MnO_2/PPy) composite was prepared by a facile solvothermal method. The conductivity polymer of PPy deposited on the surface of MnO_2 can significantly improved the electronic conductivity and accommodate the volume change. Compared with pristine β-MnO_2, the β-MnO_2/PPy exhibited excellent cycling performance and superior rate capability when used as anode for lithium-ion battery.

Introduction

Lithium-ion batteries (LIBs) have been widely applied in many portable electronic devices, and they are considered feasible power sources for electric vehicles and energy storage systems for solar and wind power.[1-4] However, as a widely used anode material for commercial LIBs, graphite could hardly meet the demand due to low theoretical capacity (372 mAh g^{-1}) and relatively poor rate capability. Therefore, it is essential to develop other anode materials with high capacity, durability, safety, and low cost.[5-9]

MnO_2 is considered as a promising anode for LIBs because of its high theoretical capacity (1232 mAh g^{-1}), nontoxicity, environmental friendly and low coast.[10-14] However, it also has obvious drawbacks such as severe pulverization and poor electric conductivity, which hamper their practical application. Therefore, extensive works have been focused on designing various structure materials to improving the conductivity and alleviating volume expansion. Until now, various MnO_2 structure materials, such as nanorods, hollow nanotubes and nanospheres have been designed with the aim to using as anode for LIBs.[15-20] Although nanostructure materials exhibited high capacities, there was no obviously to improve the electronic conductivity of the anodes, which could result in poor cycling performance and rate capability during the long discharge/charge cycles, especially at high current density. How to improve the conductivity and keep structure stable of MnO_2 is a key problem for improving battery performance. One way is to prepare MnO_2/graphite composite materials, which can provide a better connection of conductivity system. For example, different nanostructure of MnO_2, such as nanowires, nanotubes, nanoribbous and nanoflakes, have been made to composite with graphene.[21-25]

Polypyrrole (PPy) is a conductivity polymer with ion-penetrating ability, excellent mechanical properties and high electrochemical performance. It is often used to employed to act as coating layers and/or matrices to effectively enhance the structural stability of electrode materials in LIBs.[26-28] Recently, preparation of conductivity polymers coating on the surface of metal oxide as integrated electrodes is an effectively way to improving the conductivity and structure stability.[29-31] Liu et al. prepared three dimensional Fe_2O_3/PPy composite electrode with enhanced specific capacity and rate performance. It was found that this unique structure affords a highly conductive pathway for electron, a short diffusion length for Li ions, a fast mass transport channel for electrolyte, and sufficient void space for accommodating volume change during cycles.[32]

In this work, PPy film with thickness of about 5-15 nm was successfully coated on the surface of β-MnO_2 nanorods by in situ chemical oxidative polymerization method. The β-MnO_2/PPy composite can significantly improve the electronic conductivity of the electrode and effectively alleviate the intrinsic strain and stress arising from the discharge/charge cycles. At high density of 1000 mA g^{-1}, a stable capacity of 927 mAh g^{-1} was retained after 200 cycles, when used as anode for LIBs.

Experimental

Sample preparation

In a typical procedure, 0.1 g of potassium permanganate ($KMnO_4$, 99.9% purity) was added to 40 ml distilled water. After the mixture was stirred for 5 min, 2 ml of polyethylene

[a] R&D Center, China Tobacco Yunnan Industrial Co., Ltd., Kunming, 650231, China.
[b] Key Laboratory of Processing and Testing Technology of Glass and Functional Ceramics of Shandong Province, School of Material Science and Engineering, Qilu University of Technology, Jinan, 250353, China. E-mail: ligd@qlu.edu.cn

† Electronic Supplementary Information (ESI) available. See DOI: 10.1039/x0xx00000x

glycol (400) was added in droplets and vigorous stirring continued for 5 min. The solution was then transferred into a Teflon-lined stainless steel autoclave (50 ml) that was sealed and maintained at 160 °C for 5 h. The precipitates were collected and washed with distilled water and absolute ethanol. Then they were treated in air at 280 °C for 2 h to obtain the β-MnO_2 nanorods.

The as-prepared MnO_2 nanorods (20 mg) were dispersed in deionized water (100 ml) by ultrasonication for 30 min. Then, the pyrrole (≥99.5%, 50 uL) was added in the solution. After the solution was stirred for 1 h, $(NH_4)_2S_2O_8$ (0.1 M, 10 mL) solution was added in droplets and the stirring continued for 4 h. The resulting β-MnO_2/PPy was collected by filtration and washed with deionized water and ethanol.

Characterization

The obtained products were characterized by X-ray diffraction (XRD; Bruker D8 Advance, Germany). The morphologies of the samples were observed by field emission scanning electron (SEM) and transmission electron microscope (TEM) measurements, which were carried out on a JSM-7600F and a JEOL JEM 1011 TEM instrument, respectively. High-resolution transmission electron microscope (HRTEM) images were carried out on a JEOL 2010 transmission electron microscope with an accelerating voltage of 200 kV. Thermal gravimetric analysis (TGA) was carried out on a Mettler Toledo TGA/SDTA 851 thermal analyzer apparatus under air atmosphere.

Electrochemical measurements

The working electrodes were prepared with the active material, acetylene black, and carboxymethyl cellulose. The tap density of the β-MnO_2/PPy was about 1.194 g cm^{-3}. These materials were mixed together at a mass ratio of 70:20:10 with a small amount of water to produce slurry. The slurry was spread on a copper foil and dried under vacuum at 80 °C for 10 h. The obtained foil was cut into a disc with a 12 mm diameter. A Celgard 2400 membrane was used as a separator between the working electrode and the counter electrode (Li foil). The electrolyte was 1 M $LiPF_6$ in a mixture of ethylene carbonate (EC), dimethyl carbonate (DMC), and diethyl carbonate (DEC) (EC/DMC/DEC, 1:1:1 v/v/v). The working electrode, separator, electrolyte, and counter electrode were assembled into a CR2032 coin cell in an argon-filled glovebox. Cyclic voltammetry (CV) profiles (0.01–3.0 V, 0.1 mV s^{-1}) were carried out on an electrochemical workstation (CHI 660C, China). Galvanostatic discharge/charge cycles were conducted between 0.01 and 3.00 V on a battery cycler (LAND CT-2001A) at room temperature. Electrochemical impedance spectroscopy (EIS) was performed on a FRA-520 (Materials Mates Italia) connected to a Potentiostat-510 (Materials Mates Italia) over the frequency between 0.1 MHz and 0.01 Hz.

Results and discussion

Fig. 1 shows XRD pattern of the β-MnO_2/PPy and β-MnO_2 nanorods. All the diffraction peaks can be indexed to tetragonal-phase β-MnO_2 (JCPDS Card No. 24-0735). The lattice constants of the as-obtained β-MnO_2 are calculated to be a = 4.38 Å and c = 2.88 Å, which are very close to the standard values (a = 4.40 Å, c = 2.87 Å). However, the relative intensity of the (110) peak differs from the standard data owing to the preferred orientation of the crystals, as reported for several one-dimensional nanomaterials,[15,33] which is agreement with TEM observation. There are no significant difference of the diffraction peaks of the β-MnO_2/PPy composite and pristine β-MnO_2, indicating no doping reaction between PPy and β-MnO_2.

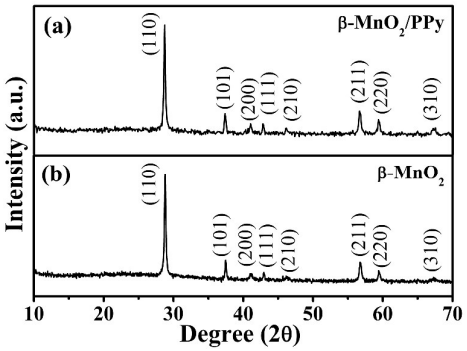

Fig. 1 XRD patterns of the (a) β-MnO_2/PPy composite and (b) β-MnO_2.

TGA is used to demonstrate the formation of PPy and determine the content of the PPy in β-MnO_2/PPy composite. As shown in Fig. 2, the β-MnO_2/PPy and PPy show a slight weight loss before 240 °C, which can is attributed to the loss of absorbed water on the material surface. From Fig. 2b, the weight loss from 240 to 600 °C can be assigned to the pyrolysis of PPy. β-MnO_2/PPy shows the same weight loss process at this temperature region. However, the weight loss ratio of β-MnO_2/PPy is slower than that of PPy, which can be ascribed to the heat transfer rate decreased in β-MnO_2/PPy composite comparing with pristine PPy. The weight kept stable after 600 °C and the content of PPy (~21.6%) in composite can be calculated according to Fig. 2a.

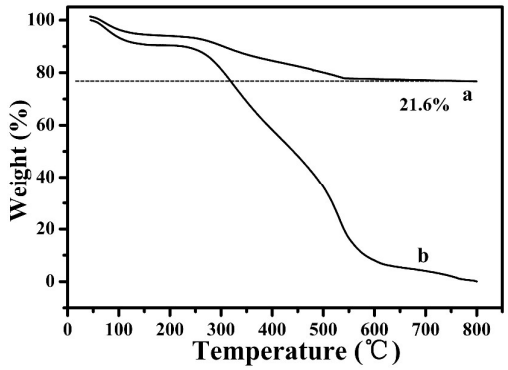

Fig. 2 TGA curves of the (a) β-MnO_2/PPy composite and (b) PPy under atmosphere.

The morphologies and nanostructures of β-MnO_2 and β-MnO_2/PPy were further investigated by TEM and HRTEM. The as-prepared β-MnO_2 nanorods have a smooth surface and they exhibited 2~10 μm in length and 30~100 nm in width (Fig. 3a). The HRTEM image shows that the interlayer spacing was about

0.30 nm, which is in accordance with the (200) plane lattice fringe of β-MnO_2. The selected-area electron diffraction (SAED) pattern (inset of Fig. 3b) corresponds to the single-crystal nature of β-MnO_2.

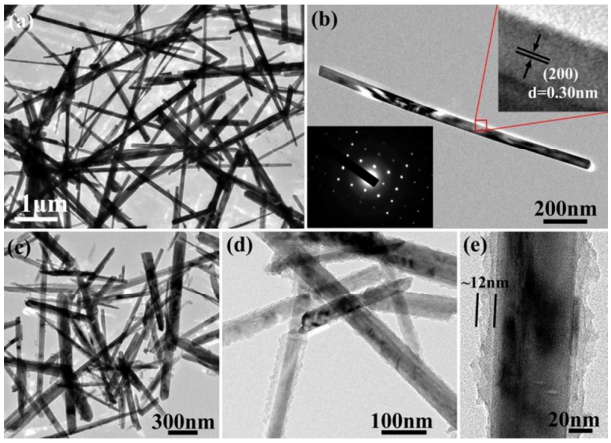

Fig. 3 (a) Typical TEM image of the β-MnO_2. (b) HRTEM image of the β-MnO_2. SAED pattern of the β-MnO_2 nanorods inset in Fig. 4b. (c~e) TEM images of the β-MnO_2/PPy composite under different magnifications.

Fig. 3c shows a typical TEM image of β-MnO_2/PPy. These composite nanorods exhibited rough outer surface comparing with pristine MnO_2 nanorods, which is believed to be the PPy layers coated on the surface of MnO_2. As shown in Fig. 3c, the thickness of PPy layers is about 5~15 nm. The clearly PPy layers on the surface of MnO_2 can be observed from Fig. 3e. The PPy compactly growth on the surface of MnO_2 nanorod and the thickness is about 12 nm. The conductivity polymer of PPy growth on the surface of MnO_2 can significantly improve the electronic conductivity and alleviate the volume change during the discharge/charge cycles. These favourable factors can result in superior cycling performance and rate capability. In this process, the MnO_2 nanorods were first synthesized by a simple solvothermal method and then make the MnO_2 homogeneous dispersed in pyrrole monomer. In presence of $(NH_4)_2S_2O_8$ under vigorous stirred, the pyrrole monomer were polymerized and growth on the surface of MnO_2 gradually.

The electrochemical properties of the β-MnO_2/PPy and β-MnO_2 were investigated by discharge/charge test, CV and EIS. Fig. 4a and b show the first three CV curves of the β-MnO_2/PPy and β-MnO_2 electrode in the voltage range of 0.01~3.0 V at a scan rate of 0.1 mV s^{-1}. The CVs of the β-MnO_2 electrode for the first three cycles (Fig. 4a) are basically consistent with reported results.[15] In the first cycle, the cathodic peaks centred at 1.02 and 0.21 V can be attributed to the reduction of MnO_2 to Mn^{2+} and then Mn^0 during lithiation process. In the third cathodic sweep, the two peaks are shifted to 1.05 and 0.30 V, indicating the structural reconstruction caused by the formation of metal particles and Li_2O. In the anodic scans, two peaks at 1.23 and 2.27 V, originating from the oxidation of Mn^0 to Mn^{2+} and Mn^{2+} to Mn^{4+}, are clearly visible and they remain in subsequent sweeps.[18] The cathodic peak of β-MnO_2/PPy electrode is centered at 0.17 V (Fig. 4b), and the other peak remains almost unchanged at 1.01 V. The shift might be attributed to the formation of a different thick gel-like polymeric layer. During the anodic scanning, two intense peaks are shifted from 1.23 and 2.27 V to 1.33 and 2.38 V, respectively, owing to the PPy shielding layer on the surface of β-MnO_2.

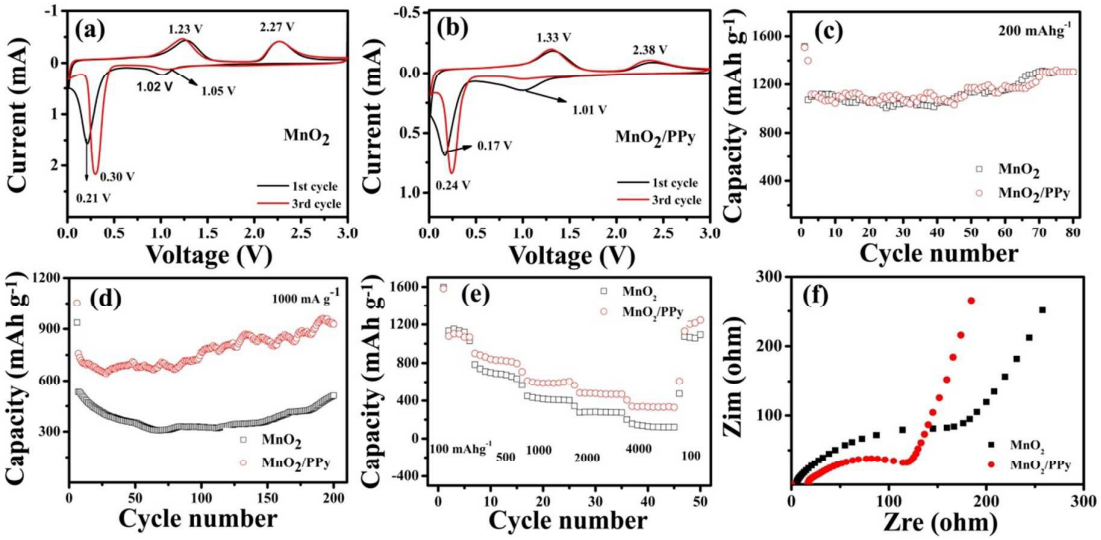

Fig. 4 CV curves of the (a) β-MnO_2 and (b) β-MnO_2/PPy composite at a scan rate of 0.1 mV s^{-1}. (c, d) Cycling performance of β-MnO_2/PPy and β-MnO_2 at 200 mA g^{-1} and 1000 mA g^{-1}. (e) Rate performance of the β-MnO_2/PPy composite and β-MnO_2 in the voltage range of 0.01–3 V. (f) Nyquist plots of the β-MnO_2 and β-MnO_2/PPy electrodes at open-circuit voltage.

Journal Name

COMMUNICATION

Fig. 4c shows the cycling performance of β-MnO_2 and β-MnO_2/PPy at a current density of 200 mA g^{-1}. The discharge capacity of the β-MnO_2/PPy composite remained at 1028 mAh g^{-1} even after 80 cycles, and the β-MnO_2 nanorods also exhibited high reversible capacity and cycling stability. At relative lower current density, the capacity and cycling performance have no large difference. When the current density increased at 1000 mA g^{-1}, a reversible capacity as high as 927 mAh g^{-1} could be restored for β-MnO_2/PPy after 200 cycles, whereas β-MnO_2 only exhibited a discharge capacity of 510 mAh g^{-1} (Fig. 4d). It was demonstrated that the rate capability and cycling performance of MnO_2/PPy is more superior to pristine MnO_2. In addition to the cycling stability, β-MnO_2/PPy exhibited better rate capability than β-MnO_2, as shown in Fig. 4e. The β-MnO_2/PPy electrode showed average discharge capacities of 1112, 838, 598, 475, and 340 mAh g^{-1} at current densities of 100, 500, 1000, 2000, and 4000 mA g^{-1}, respectively. When the current was reset to 100 mA g^{-1}, the specific capacity of the composite can return to 1213 mAh g^{-1}, demonstrating the good rate capability and cycling stability of the composite electrode. In order to further compare the cycling performance of the MnO_2-based anode materials, some relevant previous reports are summarized in Table S1. It is found that the MnO_2/PPy composite show both good cycling performance and enhanced high rate performance.

The PPy coating on the transition metal oxide greatly improved the energy density and cycle stability of the electrode because of PPy unique structural features and the synergistic effect of the materials. The PPy coating severs three main purposes. First, the PPy layers serve as the structural stabilizer, which buffer the large volume expansion, inhibit the aggregation and prevent the pulverization of MnO_2 during the cycles. Second, PPy acts as a conducting polymer coating on the surface of MnO_2, leading to enhance the conducting of MnO_2. Furthermore, the PPy layers serve as the interfacial stabilizer, preventing the exposure of MnO_2 nanospheres to the electrolyte, and thus forming a stable electrode-electrolyte interphase.[31]

The morphology changes after discharge/charge cycles of MnO_2/PPy have been observed by SEM (Fig. 5). Large-scale MnO_2/PPy nanorods can be observed before discharge/charge cycles (Fig. 5a~c). The nanorod structure of MnO_2 could also be observed after 200 cycles. However, it is found that the MnO_2 nanorods aggregated compactly, which resulted from the repetitive volume change during discharge/charge cycles. But the volume change of MnO_2/PPy was so seriously that the nanorad structure can not be observed after 500 cycles.

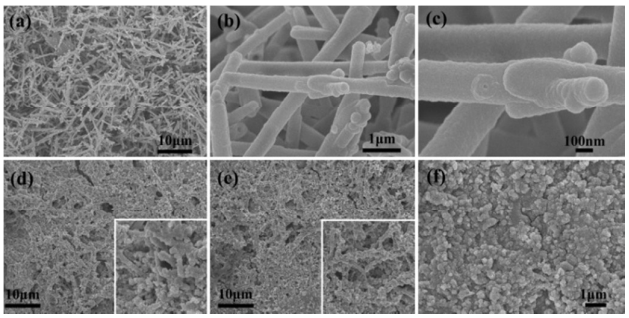

Fig. 5 (a~c) SEM images of the MnO_2/PPy before cycles. (d,e) SEM images of the MnO_2/PPy after 200 cycles. (f) SEM image of the MnO_2/PPy after 500 cycles.

EIS considered as one of the most sensitive tools for the research of electrochemical behaviour due to the surface modification.[34] The Nyquist plots of the β-MnO_2/PPy and MnO_2 at open-circuit voltage are exhibited in the Fig. 4e. The Nyquist plots are composed of a semicircle in the high frequency regions and inclined line in the low frequency region, which are relative to the charge transfer resistance (R_{ct}) and the Warburg impedance of the Li ion diffusion in the solid materials, respectively. The kinetic properties are further analyzed using the Zsimpwin software, these impedance data (Table 1) are fitted to the equivalent circuit. The diffusion coefficient values of the Li ions for diffusion into the solid electrode could be calculated using the following equation:[35,36]

$$D = 0.5(RT/AF^2Co)^2$$

$$Z_{re} = R_e + R_{ct} + \sigma\omega^{-1/2}$$

Herein, R is the gas constant, A is the surface area of the electrode, T is the absolute temperature, C is the concentration of lithium ions, F is the Faraday constant, σ is the Warburg impedance coefficient which is relative to Z_{re}, ω is the angular frequency in the low frequency, R_{ct} and R_e are the diffusion resistance and liquid resistance, respectively.

The parameters of the equivalent circuit and diffusion coefficient of the MnO_2/PPy and MnO_2 are calculated and recorded in Table 1. Comparing with EIS of MnO_2/PPy and MnO_2 (Fig. 4f), it was found that the resistance of MnO_2/PPy is lower than that of MnO_2 without PPy coating, which demonstrated the MnO_2/PPy electrode shows less resistance in the LIBs.[37] Furthermore, the Li^+ diffusion coefficient of the MnO_2/PPy electrode increases, which suggests a high Li^+ diffusion mobility in the MnO_2/PPy electrode that enhances its Li-stroge performance. The 1D nanorod structure and conductivity polymer coating can effectively facilitate electrolyte transport, shorten Li^+ diffusion path and improve the Li^+ diffusion within the MnO_2/PPy anodes.[38] Therefore,

these factors improve the cycling performance and rate capability of the batteries.

Table 1 Electrochemical impedance parameters of the MnO_2/PPy composite and MnO_2 electrodes.

Samples	R_e (Ω)	R_{ct} (Ω)	σ (Ω cm^{2}S$^{-0.5}$)	D_{Li+}(cm^2 S^{-1})
MnO_2/PPy	10.7	118.7	67.4	6.1E-14
MnO_2	11.6	172.4	148.7	1.3E-15

Conclusions

β-MnO_2/PPy composite was fabricated by simply polymerizing the pyrrole monomer over 1D β-MnO_2 nanorods. The composite exhibited significantly improved electrochemical performance because of its unique structure and conductive polymer coating. At a current density of 200 mA g^{-1}, it showed a large capacity of 1028 mAh g^{-1} after 80 cycles. Even at a rate of 1000 mA g^{-1}, a stable capacity of 927 mAh g^{-1} was retained after 200 cycles. The β-MnO_2/PPy composite exhibited excellent rate performance and good cycling stability, demonstrating that it is a promising anode material for LIBs. Modification with a conductive polymer may become a key procedure in the design of future high-power and large-capacity devices.

Acknowledgements

This work was supported by the National Natural Science Foundation of China (NSFC No. 21301102).

References

1 M. V. Reddy, G. V. Rao Subba and B. V. R. Chowdari, *Chem. Rev.*, 2013, **113**, 5364.
2 J. B. Goodenough and Y. Kim, *Chem. Mater.*, 2009, **22**, 587.
3 M. Armand and J. M. Tarascon, *Nature*, 2008, **451**, 652.
4 X. F. Wang, Y. Chen, O. G. Schmidt and C. L. Yan, *Chem. Soc. Rev.*, 2016, DOI: 10.1039/C5CS00708A.
5 Y. Chen, L. F. Liu, J. Xiong, T. Z. Yang, Y. Qin and C. L. Yan, *Adv. Funct. Mater.*, 2015, **25**, 6701.
6 Y. Hou, Y. Cheng, T. Hobson and J. Liu, *Nano Lett.*, 2010, **10**, 2727.
7 C. L. Yan, W. Xi, W. P. Si, J. W. Deng and O. G. Schmidt, *Adv. Mater.*, 2012, **25**, 539.
8 M. Sathish, T. Tomai and I. Honma, *J. Power Sources*, 2012, **217**, 85.
9 T. Z. Yang, T. Qian, M. F. Wang, X. W. Shen, N. Xu, Z. Z. Sun and C. L. Yan, *Adv. Mater.*, 2015, DOI: 10.1002/adma.201503221
10 W. M. Chen, L. Qie, Q. G. Shao, L. X. Yuan, W. X. Zhang and Y. H Huang, *ACS Appl. Mater. Inter.*, 2012, **4**, 3047.
11 C. X Guo, M. Wang, T. Chen, X. W. Lou and C. M. Li, *Adv. Energy Mater.*, 2011, **1**, 736.
12 R. Liu and S. B. Lee, *J. Am. Chem. Soc.*, 2008, **130**, 2942.
13 Y. Wang, Z. J. Han, S. F. Yu, R. R. Song, H. H. Song, K. Ostrikov and H. Y. Yang, *Carbon*, 2013, **64**, 230.
14 H. Lai, J. X. Li, Z. G. Chen and Z. G. Huang, *ACS Appl. Mater. Interfaces*, 2012, **4**, 2325.
15 X. Gu, L. Chen, Z. C. Ju, H. Y. Xu, J. Yang and Y. T. Qian, *Adv. Funct. Mater.*, 2013, **23**, 4049.
16 X. W. Guo, J. H. Han, L. Zhang, P. Liu, A. Hirata, L. Y. Chen, T. Fujita and M. W. Chen, *Nanoscale*, 2015, **7**, 15111.
17 J. J. Zhou, T. Yang, M. L. Mao, W. J. Ren and Q. H. Li, *J. Mater. Chem. A*, 2015, **3**, 12328.
18 J. b. Chen, Y. W. Wang, X. M. He, S. M. Xu, M. Fang, X. Zhao and Y. M. Shang, *Electrochim. Acta*, 2014, **142**, 152.
19 D. F. Sun, J. T. Chen, J. Yang and X. B. Yan, *CrystEngComm*, 2014, **16**, 10476.
20 Y. S. Yun, J. M. Kim, H. H. Park, J. Lee, Y. S. Huh and H. J. Jin, *J. Power Source*, 2013, **244**, 747.
21 Z. P. Li, J. Q. Wang, Z. F. Wang, Y. B. Tang and C. S. Lee, *RSC Adv.*, 2014, **4**, 54416.
22 A. P. Yu, H. W. Park, A. Davies, D. C. Higgins, Z. W. Chen and X. C. Xiao, *J. Phys. Chem. Lett.*, 2011, **2**, 1855.
23 L. Li, A. O. Raji and M. Tour, *Adv. Mater.*, 2012, **25**, 6298.
24 Y. Y. Li, Q. W. Zhang, J. L. Zhu, X. L. Wei and P. K. Shen, *J. Mater. Chem. A*, 2014, **2**, 3163.
25 Y. Cao, X. G. Lin, C. L. Zhang, C. Yang, Q. Zhang, W. Q. Hu, M. S. Zheng and Q. F. Dong, *RSC Adv.*, 2014, **4**, 301250.
26 Y. Zhao, J. X. Li, N. Wang, C. X. Wu, G. F. Dong and L. H. Guan, *J. Phys. Chem. C*, 2012, **116**, 18612.
27 J. Li and J. G. Huang, *Chem. Commun.*, 2015, **51**, 14590.
28 J. X. Li, M. Z. Zou, Y. Zhao, Y. B. Lin, H. Lai, L. H. Guan and Z. G. Huang, *Electrochim. Acta*, 2013, **111**, 165.
29 X. B. Zhong, H. Y. Wang, Z. Z. Yang, Y. B. Jin and Q. C. Jiang, *J. Power Source*, 2015, **296**, 298.
30 J. F. Zhao, S. C. Zhang, W. B. Liu, Z. J. Du and H. Fang, *Electrochim. Acta*, 2014, **121**, 428.
31 R. Q. Liu, D. Y. Li, C. Wang, N. Li, Q. Li, X. J. Lu, J. S. Spendelow and G. Wu, *Nano Energy*, 2014, **6**, 73.
32 J. L. Liu, W. W. Zhou, L. F. Lai, H. P. Yang, S. H. Lim, Y. D. Zhen, T. Yu, Z. X. Shen and J. Y. Lin, *Nano Energy*, 2013, **2**, 726.
33 W. Zhang, X. Wen and S. Yang, *Langmuir*, 2003, **19**, 4420.
34 A. Y. Shenouda and H. K. Liu, *J. Electrochem. Soc.*, 2010, **157**, A1183.
35 L. Wang, J. S. Zhao, X. M. He and C. R. Wan, *Electrochim. Acta*, 2011, **56**, 5252.
36 X. Chen, N. Q. Zhang and K. N. Sun, *J. Mater. Chem.*, 2012, **22**, 13637.
37 A. Y. Shenouda and H. K. Liu, *J. Alloys Compd.*, 2009, **477**, 498.
38 B. Jin, E. M. Jin, K. H. Park and H. B. Gu, *Electrochem. Commun.*, 2008, **10**, 1537.

The β-MnO_2/PPy composites were synthesized through in-situ chemical oxidative polymerization. The β-MnO_2/ PPy exhibit excellent cycling performance and rate capability when used as anode for LIBs.